nature cell biology

A Pumilio-induced RNA structure switch in p27-3′ UTR controls miR-221 and miR-222 accessibility

Martijn Kedde[1,4], Marieke van Kouwenhove[1,4], Wilbert Zwart[2], Joachim A. F. Oude Vrielink[1], Ran Elkon[1] and Reuven Agami[1,3,5]

Key regulators of 3′ untranslated regions (3′ UTRs) are microRNAs and RNA-binding proteins (RBPs)[1,2]. The p27 tumour suppressor is highly expressed in quiescent cells, and its downregulation is required for cell cycle entry after growth factor stimulation[3,4]. Intriguingly, p27 accumulates in quiescent cells despite high levels of its inhibitors miR-221 and miR-222 (refs 5, 6). Here we show that miR-221 and miR-222 are underactive towards p27-3′ UTR in quiescent cells, as a result of target site hindrance. Pumilio-1 (PUM1) is a ubiquitously expressed RBP that was shown to interact with p27-3′ UTR[7,8]. In response to growth factor stimulation, PUM1 is upregulated and phosphorylated for optimal induction of its RNA-binding activity towards the p27-3′ UTR. PUM1 binding induces a local change in RNA structure that favours association with miR-221 and miR-222, efficient suppression of p27 expression, and rapid entry to the cell cycle. We have therefore uncovered a novel RBP-induced structural switch modulating microRNA-mediated gene expression regulation.

MicroRNAs (miRNAs) are genes involved in normal development and in cancer, mainly by associating with 3′ untranslated regions (3′ UTRs) of messenger RNAs, regulating their expression[9,10]. In a similar manner to miRNAs, RBPs can interact with 3′ UTRs in a sequence-specific manner and can both stimulate and inhibit gene expression[1,2]. In particular, a member of the *Caenorhabditis elegans* Pumilio family (Puf-9) is required for 3′ UTR-mediated regulation of the *let-7* target *hbl-1* (ref. 11). By association with hundreds of mRNAs, many coding for cell cycle regulators, Pumilio RBPs potentially influence expression by an as yet unknown mechanism[7,8]. High levels of miR-221 and miR-222 are required in many different cancer types to inhibit the expression of *p27* (*CDKN1B*; cyclin dependent kinase inhibitor 1b) and stimulate proliferation[5,6]. p27 is a cyclin-dependent kinase inhibitor that negatively regulates cell cycle progression by association with cyclin-dependent kinase 2 (CDK2) and cyclin E complexes, resulting in the inhibition of the transition from G1 to S phase[4]. Accumulation of p27 protein is required for entry into quiescence (G0), and, on stimulation with growth factor, p27 levels must decrease to allow proper S-phase entry[3,4].

We asked whether the miR-221/miR-222 cluster is involved in p27 regulation in quiescence, because it is a negative regulator of p27 translation in many cancer cell types. We therefore examined p27 and miR-221/miR-222 levels in both quiescent and cycling BJ primary fibroblasts by RNase protection assays (RPAs), quantitative RT–PCR (qRT–PCR), and northern blot and expression array analyses. Although p27 protein level was clearly elevated in quiescent cells, *p27* mRNA and miR-221/miR-222 levels remained constant (Fig. 1a, b; Supplementary Information, Fig. S1a–d). We next inhibited miR-221 and miR-222 function by using miR-221 and miR-222 antagomirs (validated in ref. 5). Addition of miR-221 and miR-222 antagomirs, but not a control antagomir, to cycling BJ cells resulted in an increase in p27 levels (Fig. 1c). In contrast, addition of miR-221 and miR-222 antagomirs to quiescent BJ cells did not affect the level of p27 protein, suggesting that in quiescent cells miR-221 and miR-222 is less functional in suppressing its target, p27. Effective uptake of antagomirs in quiescent cells was demonstrated by a control directed against p53 short hairpin RNAs (shRNAs), in BJ-p53kd cells (Supplementary Information, Fig. S1e)[12]. Indeed, despite similar *p27* mRNA levels (Supplementary Information, Fig. S1b–d), p27 translation is increased in quiescent cells (Fig. 1d), indicating that the production of p27 protein is not inhibited in quiescent cells despite the presence of its miRNA inhibitor.

The activity of miRNAs can be dependent on accessibility to their target mRNAs[13]. To examine the association of miR-221 and miR-222 with p27-3′ UTR in quiescent and cycling cells, we immunoprecipitated endogenous Argonaute 2 (AGO2, the main component of the RNA-induced silencing complex (RISC), directing miRNA target inhibition[14]) and measured the relative amounts of associated *p27* mRNA and miR-221/miR-222. As controls we used anti-CDK4 antibody for immunoprecipitation, and both glyceraldehyde-3-phosphate dehydrogenase (GAPDH) and 18S ribosomal RNA for qRT–PCR. Although similar amounts of

[1]Division of Gene Regulation, The Netherlands Cancer Institute, Plesmanlaan 121, 1066 CX, Amsterdam, The Netherlands. [2]Division of Cell Biology II, The Netherlands Cancer Institute, Plesmanlaan 121, 1066 CX, Amsterdam, The Netherlands. [3]Centre for Biomedical Genetics UMCU, Stratenum 3.223, Universiteitsweg 100, 3584 CG Utrecht, The Netherlands.
[4]These authors contributed equally to this work
[5]Correspondence should be addressed to R.A. (e-mail: r.agami@nki.nl)

Received 01 July 2010; accepted 12 August 2010; published online 05 September 2010; DOI:10.1038/ncb2105

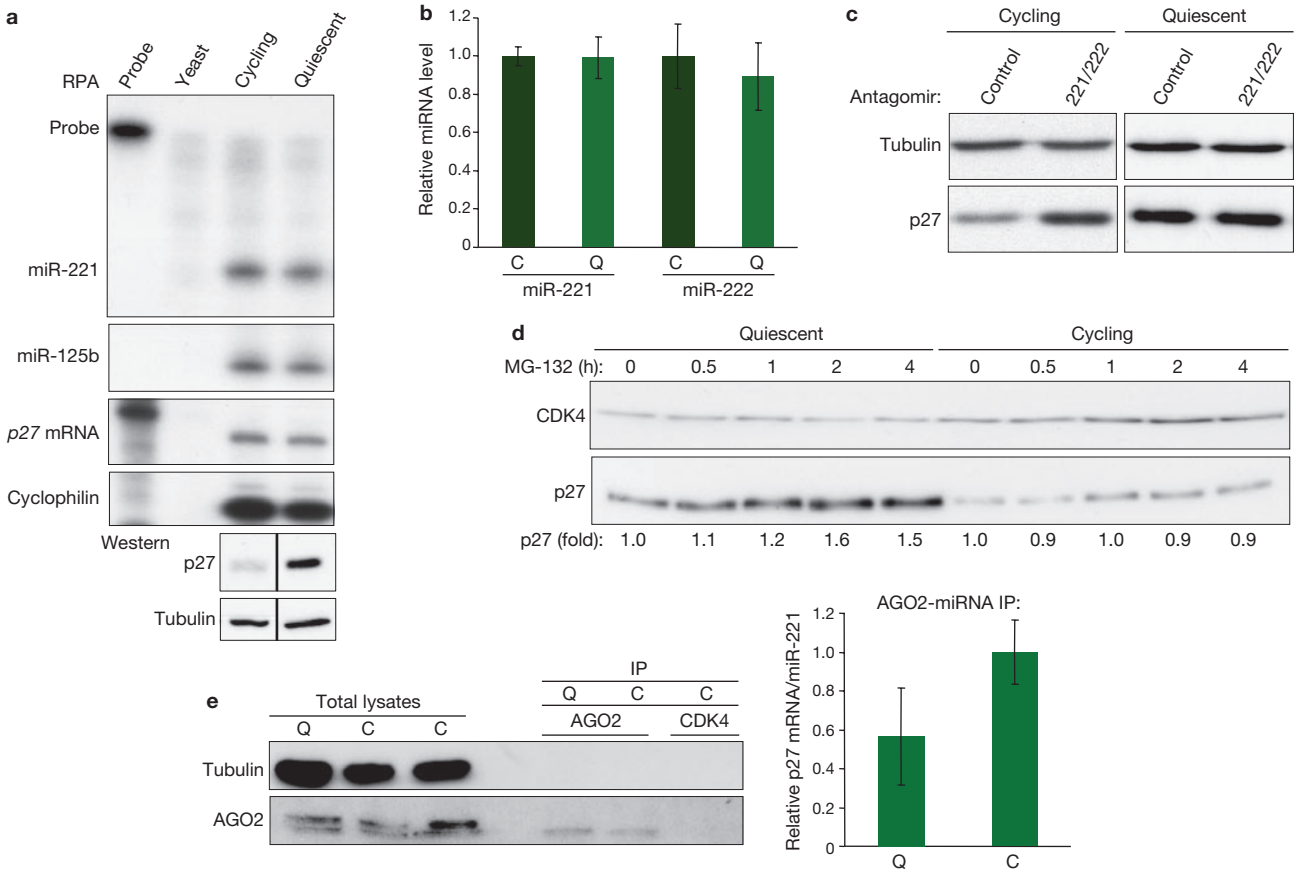

Figure 1 miR-221 and miR-222 are underactive towards p27 in quiescent cells. (**a**) RNA was extracted from quiescent and cycling BJ primary fibroblasts and was subjected to RPA analysis for p27, miR-221 and miR-125b, with cyclophilin as control. Immunoblots were performed with antibody against p27, with anti-tubulin as control. Bands were spliced together from different parts of the same blot as indicated by the line. (**b**) The amounts of miR-221 and miR-222 were measured by qRT–PCR in cycling (C) and quiescent (Q) BJ cells. Error bars represent s.d. for triplicate reactions. (**c**) Quiescent and cycling BJs were treated with cholesterol-conjugated control or miR-221/miR-222 antagomirs. Immunoblot analysis was performed as in **a**. (**d**) Quiescent and cycling BJs were treated with the proteasome inhibitor MG-132. Time points are indicated; a densitometric analysis is shown below. Immunoblot analysis was performed with antibodies against p27 and CDK4. (**e**) BJ cell extracts were used for immunoprecipitation analysis with antibodies against AGO2 and CDK4. Immunoblots were performed with antibody against AGO2, with anti-tubulin as control. The amounts of miR-221 and *p27* mRNA were measured by qRT–PCR in the immunoprecipitates. Results are presented as relative p27/miR-221 ratio. The ratio in the immunoprecipitates (IP) from cycling BJs was set to 1. Enrichment factors of miR-221 and *p27* mRNA in AGO2 immunoprecipitates over CDK4 immunoprecipitates are shown in Supplementary Information, Fig. S2b. Error bars represent s.e.m. for triplicate reactions. Uncropped images of blots are shown in Supplementary Information, Fig. S10.

AGO2 were expressed and immunoprecipitated (Fig. 1e), less *p27* mRNA was associated with AGO2–miR-221/miR-222 in quiescent cells than in cycling cells (Fig. 1e; Supplementary Information, Fig. S2a, b). Previous formaldehyde crosslinking yielded similar results (Supplementary Information, Fig. S2c). Analysis of a control miRNA (miR-29a) and its target mRNA (collagen 3A1)[15] revealed opposite association ratios, indicating the specificity of this assay (Supplementary Information, Fig. S2d). These data suggest that *p27* mRNA in cycling cells is more accessible for interaction with miR-221 and miR-222.

Recently, screens for mRNA targets of the RBP Pumilio revealed, among many genes, *p27* (refs 7, 8). The p27-3′ UTR harbours two evolutionarily conserved Pumilio recognition elements (PREs); one is located close to the miR-221 and miR-222 target sites (Fig. 2a). The human Pumilio family contains two members, PUM1 and PUM2. We knocked down PUM1, the most abundant Pumilio family member, in miR-221/miR-222-expressing HEK293 cells[13]. Immunoblot analysis revealed elevated p27 protein levels in cells transfected with either of two functional PUM1 knockdown constructs (Fig. 2b). These data suggest that PUM1 inhibits p27 expression in HEK293 cells.

Because both PUM1 and miR-221/miR-222 inhibit p27 expression, we measured the effect of PUM1 on miR-221-induced repression of a luciferase reporter gene coupled to the 3′ UTR of p27 in MCF7 cells, which endogenously express PUM1 but not miR-221 and miR-222 (ref. 13). As expected, co-transfection of miR-221 resulted in decreased luciferase activity (Fig. 2c). On knockdown of PUM1 (Supplementary Information, Fig. S3a), miR-221 function was compromised. No effect of PUM1 knockdown on the reporter was seen in the absence of miR-221 (Fig. 2c). In addition, inactivating mutations in the miR-221 and miR-222 target sites also resulted in a loss of the PUM1 knockdown effect (Supplementary Information, Fig. S3b). Moreover, mutating the PREs in p27-3′ UTR also compromised the PUM1 knockdown effect, whereas miR-221 function remained intact (Fig. 2d). The fact that PUM1 knockdown abolished miR-221 function, but loss of its binding sites on the p27-3′ UTR did not, suggests that PUM1-induced changes

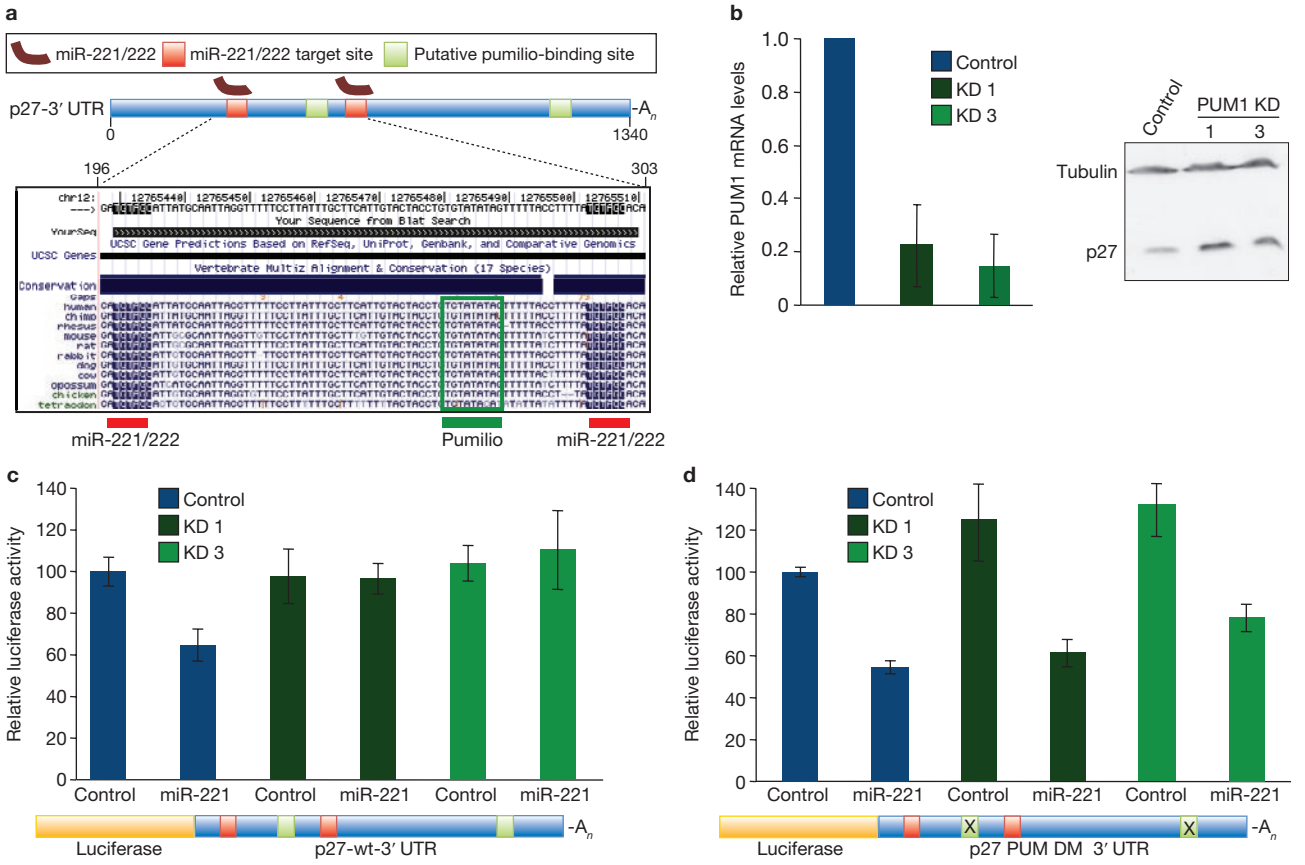

Figure 2 Pumilio is required for miR-221 and miR-222 function. (**a**) Conservation analysis of p27-3′ UTR from human to fish[25]. The positions of the binding sites for miR-221 and miR-222 and the PREs (consensus sequence 5′-UGUANAUA-3′) are marked. (**b**) HEK293 cells were transfected with shRNA constructs targeting PUM1 and control. Cells were subjected to quantitative RT–PCR for PUM1 and actin control. Error bars represent s.d. for triplicate reactions. Right: immunoblot analysis as in Fig. 1a. KD, knock-down. (**c**) MCF7 cells were co-transfected with expression vectors coding for luciferase coupled to the wild-type p27-3′ UTR, miR-221 and hTR control, and shRNA vectors against PUM1 or control. Relative luciferase activity is the ratio between firefly luciferase and *Renilla* control, adjusted to 100%. A schematic representation of the p27-3′ UTR is shown below. Error bars represent s.d. for triplicate experiments. (**d**) Luciferase assay performed as in **c**, with a luciferase construct coupled to the p27-3′ UTR mutated for the PREs. Error bars represent s.d. for triplicate experiments. Uncropped images of blots are shown in Supplementary Information, Fig. S10.

in mRNA structure are involved in regulating miR-221 function (see below). Taken together, these results indicate, first, that both PUM1 and miR-221 inhibit p27 expression post-transcriptionally through sites in p27-3′ UTR, and second, that efficient suppression of p27 expression by miR-221 requires Pumilio.

We next examined whether PUM1 RNA-binding activity is altered between quiescent and cycling cells. To test this we developed an assay to measure the RNA-binding capacity of PUM1 *in vivo* with a Cy3-tagged RNA oligonucleotide corresponding to the 5′ PRE in the p27-3′ UTR (Cy3-RNA) and a green fluorescent protein (GFP)-tagged PUM1 (Fig. 3a; Supplementary Information, Fig. S4a, b). These were microinjected into both quiescent and cycling BJ fibroblasts and revealed by fluorescent confocal microscopy. GFP–PUM1 showed a granular localization pattern, as reported previously[8]. Similar localization was observed with endogenous PUM1 (Supplementary Information, Fig. S4c). These granules are juxtaposed to P-bodies, which contain miRNAs and repressed mRNAs and are thought to be sites of translational repression[8,16,17]. We found PUM1 and AGO2 to co-localize to granules in both quiescent and cycling cells, although no direct interaction between the two could be shown (Supplementary Information, Fig. S4c, and data not shown). As a result of non-specific adhesion of Cy3-RNA oligonucleotides to chromatin, a partial nuclear localization was observed. GFP–PUM1 and Cy3-tagged wild-type RNA (Cy3-wt-RNA) showed strong co-localization in the cytosol of cycling cells (Fig. 3a, middle panel; Supplementary Information, Fig. S4b). When GFP–PUM1 and Cy3-wt-RNA were injected together into quiescent BJ cells (Fig. 3a, top panel), or when an RNA oligonucleotide with two nucleotide alterations in the PRE was injected with GFP–PUM1 into cycling cells, no co-localization was observed (Fig. 3a, bottom panel). PUM1 co-localization with Cy3-wt-RNA was specific, because it was not observed with several other RBPs (Supplementary Information, Fig. S4d, e). Direct and specific binding of PUM1 to wild-type, but not mutant, RNA is shown in immunoprecipitation-binding assays with radioactively labelled probes and PUM1–TAP (tandem affinity purification; Fig. 3b). These results indicate that the RNA binding of PUM1 is specific and its RNA-binding capacity, at least towards the p27-3′ UTR, is low in quiescent cells and high in cycling cells.

We also confirmed this conclusion by immunoprecipitations coupled to RPA of endogenous PUM1 in quiescent and cycling BJ cells. Immunoprecipitation with anti-PUM1 antibody, but not an anti-CDK6 control, from cycling BJ cells confirmed binding of PUM1 to *p27* mRNA (Fig. 3c; quantification is shown in Supplementary Information, Fig. S4f). The cyclophilin RNA-negative control was not enriched in

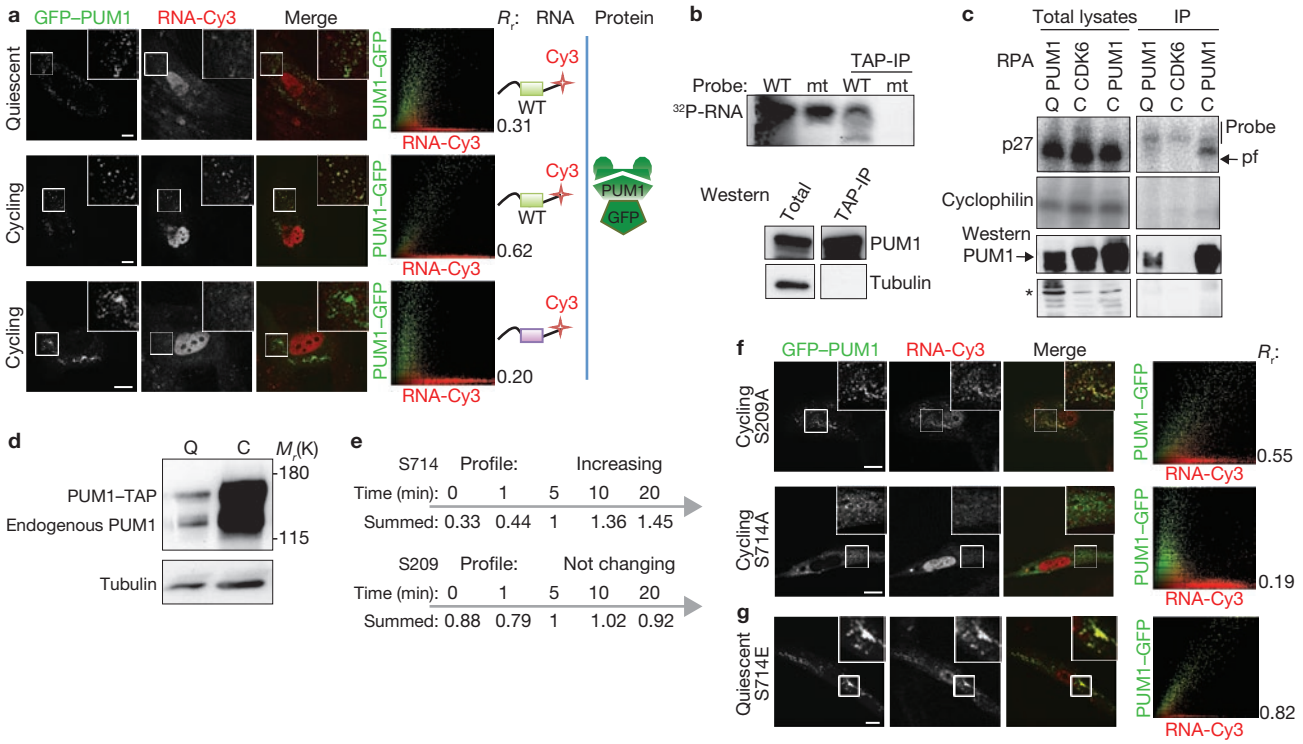

Figure 3 PUM1 RNA-binding activity is enhanced in cycling versus quiescent cells. (**a**) Quiescent or cycling BJ primary fibroblasts were microinjected with GFP–PUM1 constructs and a Cy3-labelled RNA. After incubation overnight, cells were fixed and revealed by confocal laser scanning microscopy (CLSM). Co-localization is shown in the merge panel, and the correlations between GFP and Cy3 signals within the same cell were ascertained with a scatter plot. Representative pictures are shown. Insets: enlargements of the highlighted areas. Pearson's correlation coefficients (R_r) are shown in the scatter plots. wt, wild-type; mut, mutant. Scale bar, 10 μm. (**b**) Binding assay of immunoprecipitated PUM1–TAP from HEK293 cells and ^{32}P-labelled wild-type (wt) and mutant (mt) p27 RNA. Gel image displays both unbound and bound probes. Total lysate and immunoprecipitate (TAP-IP) were analysed by immunoblotting with antibody against PUM1, with anti-tubulin as control. (**c**) RPA for *p27* mRNA and cyclophilin negative control was performed on immunoprecipitates of PUM1 complexes and of CDK6 control from cycling (C) and quiescent (Q) BJ cells. pf, protected fragment. Quantification is shown in Supplementary Information, Fig. S4f. Total lysates and immunoprecipitates (IP) were analysed by immunoblotting with antibody against PUM1. Asterisk, loading control. (**d**) Immunoblot analysis of endogenous and overexpressed PUM1 on growth factor stimulation with antibody against PUM1, with anti-tubulin as control. (**e**) Data adapted from the PHOSIDA phosphorylation site database showing the phosphorylation of PUM1 at Ser 209 and Ser 714 along the course of stimulation with epidermal growth factor (in minutes). (**f**) Cycling BJ cells were microinjected with inactivated phospho-mutants of GFP–PUM1 (S209A, S714A) in combination with Cy3-tagged RNA. The experiment was performed as in **a**. (**g**) Quiescent BJ cells were microinjected with a phospho-mimic mutant (S714E) of GFP–PUM1, in combination with Cy3-tagged *p27* RNA. The experiment was performed as in **a**. Uncropped images of blots are shown in Supplementary Information, Fig. S10.

the immunoprecipitations, indicating the specificity of PUM1 binding. In contrast, in quiescent BJ cells no *p27* mRNA was detected in PUM1 immunoprecipitation. Immunoblot analysis revealed higher levels of endogenous PUM1 in cycling BJ cells than in quiescent cells (Fig. 3c). This effect was observed with both endogenous and stable exogenous tagged PUM1 (Fig. 3d), indicating post-translational modifications. Taken together, our observations show that, on cell cycle entry from quiescence, PUM1 levels increase and its RNA-binding activity is turned on.

A study of phosphorylated proteins in HeLa cells reported unchanged phosphorylation of PUM1 Ser 209 on stimulation with epidermal growth factor, whereas Ser 714 phosphorylation was rapidly increased up to about fivefold (Fig. 3e)[18,19]. To examine whether these phosphorylation sites affect the RNA-binding activity of PUM1 in cycling cells, GFP–PUM1 phospho-mutants (Supplementary Information, Fig. S4a) were microinjected together with the Cy3-RNA oligonucleotides into cycling BJ cells. Mutation of Ser 714 to alanine (S714A) decreased the RNA-binding activity of PUM1 for Cy3-wt-RNA in cycling cells (Fig. 3f, lower panel), whereas the S209A mutant was as active as wild-type PUM1 (Fig. 3f, upper panel). Furthermore, a phospho-mimic mutation of Ser 714 to glutamic acid (S714E) showed persistent RNA-binding activity in quiescent cells (Fig. 3g). In contrast, the RNA-binding domain of PUM1 (GFP–PUM1(HD); HD: homology domain) is mostly nuclear, and the cytoplasmic fraction does not co-localize to Cy3-wt-RNA (Supplementary Information, Fig. S4g). This suggests that residues outside the HD domain are essential for cytoplasmic localization and binding specificity. Although the results above do not exclude the involvement of other modification events in the activation process of PUM1, they suggest that both PUM1 upregulation and phosphorylation of Ser 714 in response to stimulation with growth factor are necessary and sufficient to increase the RNA-binding activity of PUM1 in BJ fibroblasts.

Next we examined the effect of Pumilio on endogenous p27 expression and cell cycle re-entry from quiescence. PUM1 knockdown resulted in a delayed re-entry into the cell cycle from quiescence (Supplementary Information, Fig. S5a) despite modest differences in p27 levels (see below); this can be explained by haploinsufficiency of p27 (ref. 20). We noticed that the levels of PUM2, a homologue of PUM1 that is also expressed in BJ and HEK293 cells, increased when PUM1 was suppressed by RNA-mediated

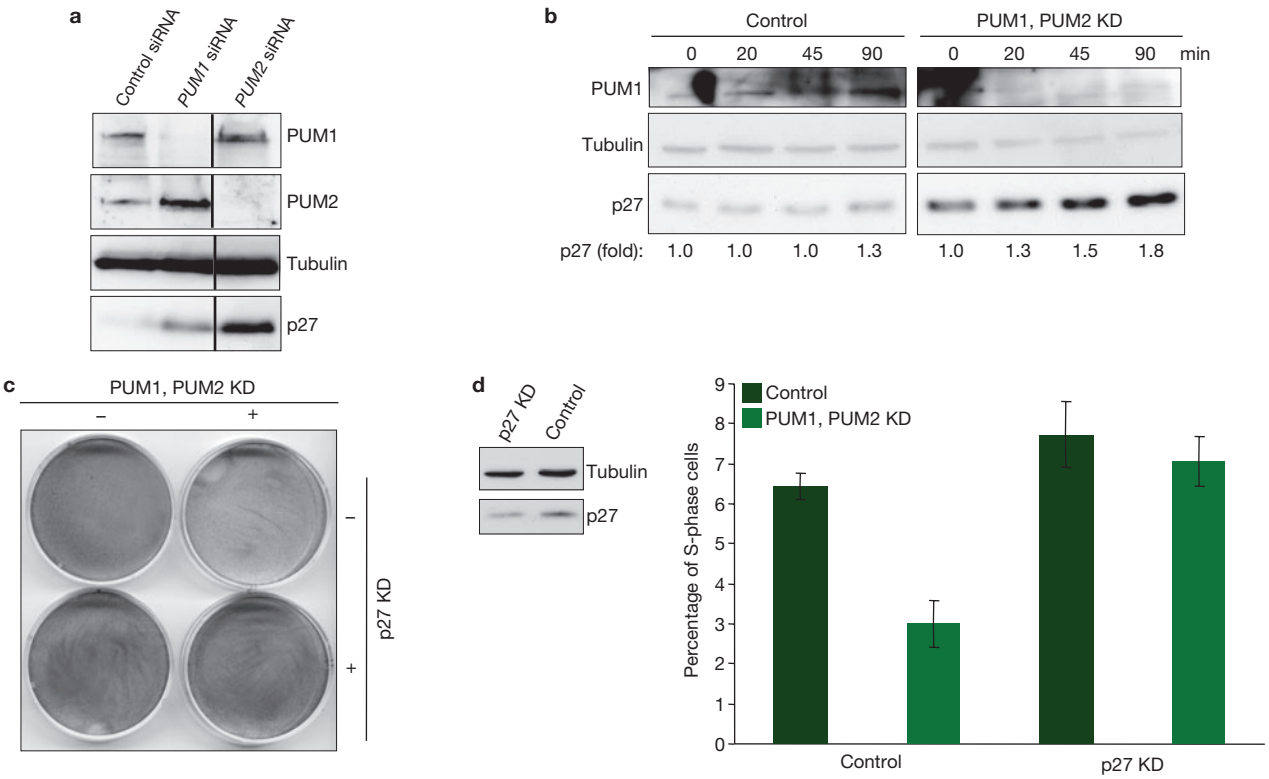

Figure 4 Pumilio regulates p27-dependent cell cycle re-entry from quiescence. (**a**) HEK293 cells were transiently transfected with *PUM1* siRNA, *PUM2* siRNA and scrambled control siRNA, and immunoblot analysis was performed with antibodies against PUM1, PUM2 and p27, with anti-tubulin as control. (**b**) HEK293 cells transfected with *PUM1*- and *PUM2*-siRNA, or control, were treated with the proteasome inhibitor MG-132. A densitometric analysis at the indicated time points is shown below. Immunoblot analysis was performed as in **a**. (**c**) HEK293 cells were transfected with shRNA vectors against p27 or control, and with either *PUM1*- and *PUM2*-siRNA or control siRNA. After 3 days the cell densities were revealed by staining with Coomassie blue. (**d**) Wild-type BJ cells and BJ cells containing a stable p27 knockdown were transfected with either *PUM1*- and *PUM2*-siRNA or control siRNA, and deprived of growth factors for 72 h. After 16 h of subsequent stimulation with growth factor, the percentage of cells in S phase was determined by flow cytometric analysis of bromodeoxyuridine incorporation. The percentage of cells in G1 and G2/M are shown in Supplementary Information, Fig. S5c. Error bars represent s.d. for three independent experiments. Immunoblot analysis of BJ cells stably expressing p27 KD or control was performed with antibody against p27, with anti-tubulin as control. Uncropped images of blots are shown in Supplementary Information, Fig. S10.

interference (Fig. 4a and data not shown). The presence of two PREs in the 3′ UTR of PUM2 could explain this[7]. Suppression of PUM2, like that of PUM1, led to an increase in p27 levels and a comparable delay in cell cycle re-entry, suggesting a redundant activity with PUM1 (Supplementary Information, Fig. S5b). Knockdown of both PUM1 and PUM2 significantly increased p27 protein levels by elevating translation (Fig. 4b) and halted proliferation (Fig. 4c). Knockdown of PUM1 and PUM2 in BJ cells caused a delayed entry into S phase on stimulation with growth factor, whereas BJ cells containing a stable p27 knockdown were insensitive to the loss of PUM1 and PUM2 (Fig. 4d; Supplementary Information, Fig. S5c). These results indicate that Pumilio proteins control cell cycle re-entry in response to growth factors, and that this function is in part mediated by controlling p27 expression.

Using the secondary structure prediction RNAfold software (Vienna RNA package version 1.8.3)[21], we noticed that the PRE and the miR-221 and miR-222 target site could form a stem-loop structure with considerable base-pair probability (Fig. 5a; Supplementary Information, Fig. S6). We therefore speculated that PUM1-binding to the PRE favours opening of the stem-loop structure, allowing miR-221 and miR-222 to gain access to the p27-3′ UTR in cycling cells. To study changes in RNA secondary structure *in vivo*, we tagged RNA oligonucleotides containing the p27-3′ UTR PRE and the proximal miR-221/miR-222-binding site, with both 3′ (fluorescein) and 5′ (Cy3) fluorophores. On microinjection of this RNA, the fluorescein lifetime in cycling BJ cells was significantly longer than in quiescent cells, as a result of decreased energy transfer (FRET; fluorescence resonance energy transfer) to the Cy3 fluorophore (Fig. 5b). This suggests an increased distance between the two fluorophores and thus a more open conformation of the stem-loop structure in cycling cells. To examine the potential differences in donor-fluorophore lifetime and to test the specificity of this assay, we microinjected mutant RNAs with strong and weak predicted secondary structures (Fig. 5b; Supplementary Information, Fig. S7). A PRE mutant RNA that was energetically more stable than the wild-type RNA (strong mutant) showed a short fluorescein lifetime in both quiescent and cycling cells, suggesting an unchanged, closed, RNA conformation. In contrast, an energetically weak structured RNA mutated in the miRNA site (weak mutant) maintained a longer fluorescein lifetime in both quiescent and cycling cells, suggesting an open conformation in both conditions. Because the changes in FRET observed with the wild-type RNA were within the range indicated by the mutant RNAs, our results imply that the measured changes in FRET represent actual structural differences. We also tested changes in luciferase–p27-3′ UTR reporter activity on mutation of either PUM binding site with strong or weak complementarity to the miRNA sites. Whereas the weak mutant of both PUM sites permitted

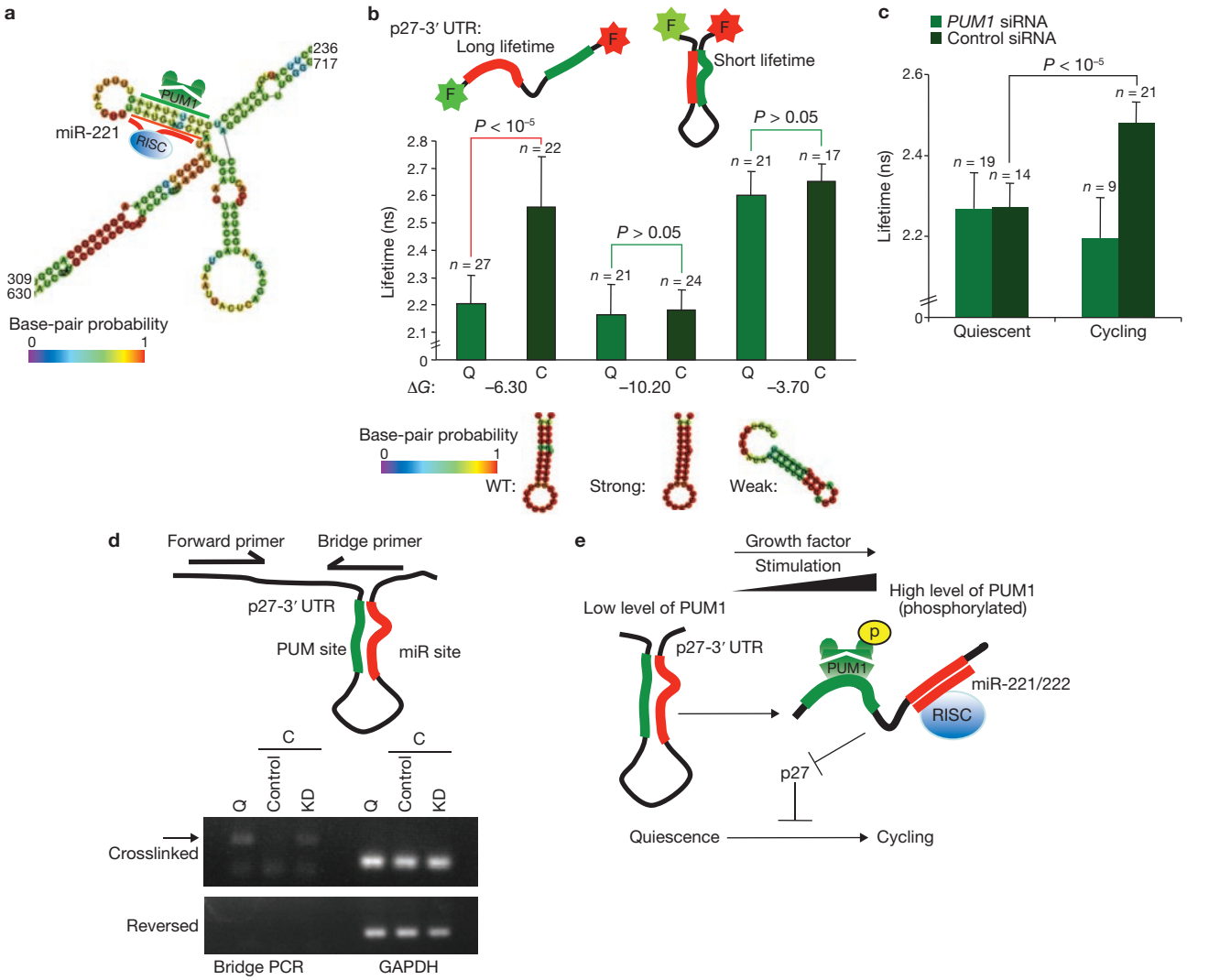

Figure 5 Pumilio binding alters local p27-3′ UTR structure and miR-221 and miR-222 accessibility. (**a**) Schematic representation of the conformation of a region of the p27-3′ UTR containing a PRE and a miR-221/miR-222 site as predicted by RNAfold software. Base-pair probability is indicated in the key. (**b**) Quiescent (Q) and cycling (C) BJ cells were microinjected with short RNAs containing the p27-3′ UTR-PRE and the proximal miR-221/miR-222-binding site, and tagged with both 3′ (fluorescein) and 5′ (Cy3) fluorophores. The amount of conformational free energy (ΔG in kcal mol^{-1}) is listed for the wild-type (WT) and the two mutant short RNAs (named accordingly 'strong' and 'weak'). Differences in Cy3 fluorophore lifetime (in ns) due to FRET are shown, and *P* values are calculated for the differences in lifetime. Error bars represent s.d. (**c**) BJ cells were transfected with *PUM1* siRNA and control siRNA and microinjected with the wild-type short RNA as in **b**. Error bars represent s.d. (**d**) Model representing part of the p27-3′ UTR, indicating the sequences recognized by the bridge primer used for RT and PCR. Ethidium-bromide-stained gels of PCRs performed on bridge or GAPDH reverse primer-primed cDNA from crosslinked or crosslink-reversed RNA isolated from quiescent (Q), cycling (C) and cycling PUM1 and PUM2 knockdown (KD) BJ cells. (**e**) Model proposing a role for Pumilio RBPs in mammalian somatic cells. See the text for details. Uncropped images of blots are shown in Supplementary Information, Fig. S10.

miRNA-mediated repression, altering either or both of the PUM sites to strong mutants abrogated miRNA activity (Supplementary Information, Fig. S8). These results suggest a functional interaction between Pumilio and miR-221/miR-222 through their binding sites on the p27-3′ UTR and indicate that both Pumilio sites in p27-3′ UTR may contribute to the miRNA inhibitory structure *in vivo*.

On PUM1 knockdown in quiescent BJ cells, donor lifetime was not affected when compared with transfection of control siRNAs, which is consistent with an inactive state of PUM1 (Fig. 5c). In contrast, knockdown of PUM1 in cycling cells abolished the increase in donor lifetime, suggesting that the changes in conformation observed with the wild-type oligonucleotide are dependent on PUM1 protein. These results are supported by *in vivo* crosslinking of BJ cells and RT–PCR with a primer designed to detect the structured RNA loop specifically. A PCR product indicating a closed p27-3′ UTR conformation was observed in quiescent cells and in PUM1 and PUM2 knockdown cells but not in cycling cells (Fig. 5d; Supplementary Information, Fig. S9).

Taken together, our results provide evidence in support of a model in which, on stimulation by growth factors, Pumilio levels are increased and RNA-binding activity is further enhanced by phosphorylation inducing a conformational change in the p27-3′ UTR (Fig. 5e). These changes permit a more efficient binding of miR-221 and miR-222 specifically to their target sites on the p27-3′ UTR and tuning of cell cycle progression by repressing p27 expression. In addition, miRNA upregulation in

response to growth factors has been reported in cancer cells, resulting in global target downregulation, implying distinct modes of regulation to achieve target specificity[22]. Our results reveal a highly conserved, specific case of complementarity of an RBP target motif to a miRNA-binding site. To our knowledge, this is the only demonstration of an RBP that modulates miRNA activity by inducing a local structural switch in mRNA. Considering the generally high conservation of some 3′ UTR regions, we expect that other RBPs may be found to modulate miRNA regulation of other genes in a similar manner. □

METHODS

Methods and any associated references are available in the online version of the paper at http://www.nature.com/naturecellbiology/

Note: Supplementary Information is available on the Nature Cell Biology website.

ACKNOWLEDGEMENTS

We thank all members of the Agami laboratory for technical help and discussions. We also thank André Gerber for constructs, Kees Jalink for advice on fluorescence lifetime imaging microscopy measurements, and R. B. Israel for assistance with statistical analysis. This work was supported by the EURYI (European research young investigator award), ERC (European Research Council), KWF (koningin wilhelmina fonds; Dutch cancer foundation) and Horizon-NWO (Nederlandse Organisatie voor Wetenschappelijk Onderzoek; R.A.) and an EMBO long-term fellowship (R.E.).

AUTHOR CONTRIBUTIONS

M.K. and M.v.K. performed most of the experimental work. R.A. supervised the project. W.Z. performed fluorescence lifetime imaging microscopy and confocal laser scanning microscopy analyses. J.O.V. provided technical assistance. R.E. performed bioinformatical analyses. M.K., M.v.K. and R.A. wrote the manuscript.

COMPETING FINANCIAL INTERESTS

The authors declare no competing financial interests.

Published online at http://www.nature.com/naturecellbiology
Reprints and permissions information is available online at http://npg.nature.com/reprintsandpermissions/

1. Filipowicz, W., Bhattacharyya, S. N. & Sonenberg, N. Mechanisms of post-transcriptional regulation by microRNAs: are the answers in sight? *Nat. Rev. Genet.* **9,** 102–114 (2008).
2. Kedde, M. & Agami, R. Interplay between microRNAs and RNA-binding proteins determines developmental processes. *Cell Cycle* **7,** 899–903 (2008).
3. Hengst, L. & Reed, S. I. Translational control of p27Kip1 accumulation during the cell cycle. *Science* **271,** 1861–1864 (1996).
4. Chu, I. M., Hengst, L. & Slingerland, J. M. The Cdk inhibitor p27 in human cancer: prognostic potential and relevance to anticancer therapy. *Nat. Rev. Cancer* **8,** 253–267 (2008).
5. le Sage, C. *et al.* Regulation of the $p27^{Kip1}$ tumor suppressor by miR-221 and miR-222 promotes cancer cell proliferation. *EMBO J.* **26,** 3699–3708 (2007).
6. Lotterman, C. D., Kent, O. A. & Mendell, J. T. Functional integration of microRNAs into oncogenic and tumor suppressor pathways. *Cell Cycle* **7,** 2493–2499 (2008).
7. Galgano, A. *et al.* Comparative analysis of mRNA targets for human PUF-family proteins suggests extensive interaction with the miRNA regulatory system. *PLoS ONE* **3,** e3164 (2008).
8. Morris, A. R., Mukherjee, N. & Keene, J. D. Ribonomic analysis of human Pum1 reveals *cis-trans* conservation across species despite evolution of diverse mRNA target sets. *Mol. Cell. Biol.* **28,** 4093–4103 (2008).
9. Kloosterman, W. P. & Plasterk, R. H. The diverse functions of microRNAs in animal development and disease. *Dev. Cell* **11,** 441–450 (2006).
10. Voorhoeve, P. M. & Agami, R. Classifying microRNAs in cancer: the good, the bad and the ugly. *Biochim. Biophys. Acta* **1775,** 274–282 (2007).
11. Nolde, M. J., Saka, N., Reinert, K. L. & Slack, F. J. The Caenorhabditis elegans *pumilio* homolog, *puf-9*, is required for the 3′UTR-mediated repression of the *let-7* microRNA target gene, *hbl-1*. *Dev. Biol.* **305,** 551–563 (2007).
12. Brummelkamp, T. R., Bernards, R. & Agami, R. Stable suppression of tumorigenicity by virus-mediated RNA interference. *Cancer Cell* **2,** 243–247 (2002).
13. Kedde, M. *et al.* RNA-binding protein Dnd1 inhibits microRNA access to target mRNA. *Cell* **131,** 1273–1286 (2007).
14. Pillai, R. S. *et al.* Inhibition of translational initiation by Let-7 microRNA in human cells. *Science* **309,** 1573–1576 (2005).
15. van Rooij, E. *et al.* Dysregulation of microRNAs after myocardial infarction reveals a role of miR-29 in cardiac fibrosis. *Proc. Natl Acad. Sci. USA* **105,** 13027–13032 (2008).
16. Leung, A. K., Calabrese, J. M. & Sharp, P. A. Quantitative analysis of Argonaute protein reveals microRNA-dependent localization to stress granules. *Proc. Natl Acad. Sci. USA* **103,** 18125–18130 (2006).
17. Kedersha, N. *et al.* Stress granules and processing bodies are dynamically linked sites of mRNP remodeling. *J. Cell Biol.* **169,** 871–884 (2005).
18. Gnad, F. *et al.* PHOSIDA (phosphorylation site database): management, structural and evolutionary investigation, and prediction of phosphosites. *Genome Biol.* **8,** R250 (2007).
19. Olsen, J. V. *et al.* Global, *in vivo*, and site-specific phosphorylation dynamics in signaling networks. *Cell* **127,** 635–648 (2006).
20. Fero, M. L., Randel, E., Gurley, K. E., Roberts, J. M. & Kemp, C. J. The murine gene $p27^{Kip1}$ is haplo-insufficient for tumour suppression. *Nature* **396,** 177–180 (1998).
21. Hofacker, I. L. Vienna RNA secondary structure server. *Nucleic Acids Res.* **31,** 3429–3431 (2003).
22. Medina, R. *et al.* MicroRNAs 221 and 222 bypass quiescence and compromise cell survival. *Cancer Res.* **68,** 2773–2780 (2008).

METHODS

Constructs and antibodies. MiR-Vec constructs and the pGL3-p27-3′ UTR and miR mutants were described previously[5,23]. The PREs in the p27-3′ UTR were mutated (weak) to the following sequences using the Stratagene multisite-directed mutagenesis kit: PRE1, 5′-tgtatata-3′ to 5′-ggtatgta-3′; PRE2, 5′-tgtacata-3′ to 5′-ggtacgta-3′ (strong mutants are shown below). Constructs for RPA detection of hTR, cyclophilin, p27 and miR-221 were described previously[13]; the RPA probe sequence for miR-125b was 5′-CUCAGUCCCUGAGACCCUAACUUGUGAUGUUU-3′. Probes were prepared in accordance with the manufacturer's instructions (Ambion mirVana probe construction kit). shRNA for p27 was described previously[5]; the shPUM1.1 sequence was 5′-AATCCAACATGTACTGGAGCA-3′, the shPUM1.3 sequence was 5′-AACAGACCACCCCACAGGCTC-3′, the shPUM1.4 sequence was 5′-AATTCAGCTAATCAACAGACC-3′; these were cloned in pRETRO-SUPER. siRNAs ordered from Ambion were against PUM1 (no. 138317), PUM2 (no. 138319) and a scrambled control (5′-CUGUAGCCGUAUCAAGUCGUUCCUGTT-3′) from Invitrogen. The PUM1–TAP construct was a gift from A. Gerber. The GFP–PUM1(HD) and GFP–RBP constructs were made by cloning the cDNA into the Clontech eGFP vector; mutants were made with the Stratagene multisite-directed mutagenesis kit. All constructs were sequence-verified. The Cy3-wt-RNA oligonucleotide (5′-ACUACCUGUGUAUAUAGUUUUU-3′) and the Cy3-mt-RNA oligonucleotide (5′-ACUACCUCUCCAUAUAGUUUUU-3′) were labelled 3′ (Dharmacon). Labelled RNA oligonucleotides (3′ (fluorescein) and 5′ (Cy3)) used for FLIM were wild-type (5′-CUGUGUAUAUAGUUUUUACCUUUUAUGUAGCACAU-3′), strong mutant (5′-CUGUGCACAUAGUUUUUACCUUUUAUGUAGCACAU-3′) and weak mutant (5′-CUGUGUAUAUAGUUUUUACCUUUUAGGUCGGAGAU-3′) (Dharmacon).

Antibodies used were AGO2 (Transduction Labs and Abcam), actin (Abcam), p27 (Transduction Labs), CDK4 (C22), p53 (DO1) and CDK6 (Santa Cruz), PUM1 and PUM2 (Bethyl Labs), tubulin (YL1/2 ECACC), rabbit GFP and bromodeoxyuridine (Dako).

Cell culture, transfections, dual luciferase activity analysis and cell cycle profile analysis. HEK293, MCF7 and BJ primary fibroblast cells were cultured in DMEM supplemented with 10% heat-inactivated fetal calf serum (FCS) in 5% CO_2 at 37 °C. HEK293 cells were transiently transfected by using calcium phosphate precipitation. MCF7 cells were transfected with Fugene (Roche) for luciferase analysis with 10 ng of reporter, 5 ng of *Renilla* control plasmid, 250 ng of either miR-Vec or miR-Vec control, and 250 ng of knockdown construct for PUM1 or control. Dual luciferase activity assays were performed 72 h after transfection in accordance with the manufacturer's instructions (Promega). BJ cells were transfected with siRNAs in a final concentration of 50 nM with the use of Dharmafect reagent (Dharmacon), in accordance with the manufacturer's instructions. To obtain quiescent BJ cells, cells were cultured for 72 h in DMEM containing 0.25% FCS. Antagomir sequences were described previously[5] and applied to the cells overnight at a final concentration of 15 μM. The proteasome inhibitor MG-132 was from Sigma, used at a final concentration of 10 μM. For cell cycle profile analysis, quiescent BJs were stimulated with growth factors. Cell cycle analysis was performed as described previously[24].

Immunoprecipitation, immunoblotting, RNAse protection assays and qRT–PCR analysis. PUM1 and AGO2 were immunoprecipitated from BJ cell extracts with GammaBind G Sepharose (GE Healthcare). Beads were preblocked with yeast tRNA (Invitrogen) and RNase-free BSA (Ambion) and then washed; extracts were sonicated and cleared in lysis buffer (100 mM KCl, 10 mM Tris-HCl pH 7.5, 0.1% Nonidet P40, 0.5% Tween 20, 5 mM $MgCl_2$, 2 mM β-glycerophosphate, 0.5 mM dithiothreitol, protease inhibitor mixture (Roche Applied Science) and RNAse-OUT (Invitrogen). Extracts were incubated for 4 h with antibodies against AGO2, CDK4, CDK6 or PUM1 (1 μg per immunoprecipitation) in a tumbler placed at 4 °C. Thereafter, beads were washed and a 10% aliquot was used for immunoblot analysis; from the remainder, RNA was extracted (Trizol, Invitrogen) to be subjected to RPA or qRT–PCR analysis. PUM1–TAP was precipitated from transiently transfected HEK293 cells by using rabbit IgG Sepharose (Sigma) in lysis buffer with 125 mM NaCl instead of KCl as described above. Beads were washed and incubated for 20 min with ^{32}P-labelled oligonucleotides (wild-type and mutant, described above) at 30 °C. Beads were washed, and bound RNA and proteins were revealed on gel.

For immunoblot analysis, extracts were separated on 10% SDS–PAGE gels, and transferred to Immobilon-P membranes (Millipore). Western blots were developed with Supersignal (Pierce) or by enhanced chemiluminescence (ECL; Amersham Biosciences) and exposed to film (Kodak). Densitometric analysis was performed with AIDA software (Raytest).

RPAs for p27 and cyclophilin were performed with the HybSpeed RPA and MAXIscript kits (Ambion) as described[13]. For miRNAs, we used mirVana kits (Ambion) in accordance with the manufacturer's instructions[13]. Northern analysis was performed with standard protocols and RPA probe for p27.

For mRNA qRT–PCR, cDNA (from 3 μg RNA) was synthesized with SuperScript III and primed with oligo(dT) in accordance with the manufacturer's instructions (Invitrogen). For combined miRNA and mRNA qRT–PCR, about 100 ng of input RNA and 20% of immunoprecipitated RNA was used for cDNA synthesis with random primers from a Taqman High Capacity cDNA kit (Applied Biosystems), in accordance with the manufacturer's instructions. Primers for qPCR were PUM1 (5′-AAAAACCTGAGAAGTTTGAATTGT-3′ (forward) and 5′-GCAAGACCAAAAGCAGAGTTG-3′ (reverse)) and COL3A1 (5′-AACACGCAAGGCTGTGAGACT-3′ (forward) and 5′-GCCAACGTCCACACCAAATT-3′ (reverse)); p27, GAPDH and β-actin primers were as described[13]. QPCR primers for miR-221, miR-222, miR-29a, GAPDH and 18S were from Applied Biosystems. Analysis was performed with SYBR Green PCR master mix or TaqMan UNG master mix (Applied Biosystems) and Chromo 4 system (Bio-Rad Laboratories).

Crosslink bridge RT–PCRs were performed with bridge reverse (5′-CTTCCCCAAAGTTTATAGGTAG-3′) and GAPDH reverse primer; PCR forward primer was 5′-TATAAGCACTGAAAAACAACAACAC-3′. BJ cells were crosslinked for 15 min with 1% formaldehyde (Sigma), inactivated with 330 mM glycine (Sigma), sonicated and cleared. Cleared lysate was treated for 1 h with proteinase K (Invitrogen) at 37 °C and inactivated with phenylmethylsulphonyl fluoride (Sigma). RNA was extracted, and reverse crosslinking was performed for 1 h at 70 °C.

Fluorescence lifetime imaging microscopy (FLIM). Before FLIM experiments, cells were grown on coverslips and microinjected with RNA labelled 3′ with fluorescein and 5′ with Cy3. Subsequently, cells were mounted in bicarbonate-buffered saline (140 mM NaCl, 5 mM KCl, 1 mM $MgCl_2$, 1 mM $CaCl_2$, 23 mM $NaHCO_3$, 10 mM glucose, 10 mM HEPES at pH 7.3) in a heated tissue-culture chamber at 37 °C under 5% CO_2. FLIM experiments were performed on a Leica inverted DM-IRE2 microscope equipped with a Lambert Instruments frequency domain lifetime attachment (Leutingewolde), controlled by the vendor's LI FLIM software. Fluorescein was excited with about 4 mW of 488-nm light from a light-emitting diode modulated at 40 MHz; emited light was collected at 490–550 nm with an intensified charge-coupled-device camera (CoolSNAP HQ; Roper Scientific). To calculate the fluorescein lifetime, the intensities from 12 phase-shifted images (modulation depth about 70%) were fitted with a sinus function, and lifetimes were derived from the phase shift between excitation and emission. Differences in lifetimes were assigned *P* values with Student's *t*-test.

CLSM analysis. For CLSM analysis, BJs were microinjected with GFP–PUM1 or its mutants, in combination with Cy3-labelled RNA. After expression of the GFP–PUM1 overnight, cells were fixed with 3.7% formaldehyde in PBS, and coverslips were mounted in Vectashield mounting medium (Vector Laboratories). The specimens were imaged with a Leica TCS SP2 System equipped with a 63× oil-immersion objective. Endogenous stainings for PUM1 and AGO2 were performed in accordance with the manufacturer's instructions. Scatter plots for co-localization analysis were generated with ImageJ WCIF software (http://www.uhnresearch.ca/wcif).

23. Voorhoeve, P. M. *et al*. A genetic screen implicates miRNA-372 and miRNA-373 as oncogenes in testicular germ cell tumors. *Cell* **124,** 1169–1181 (2006).
24. Duursma, A. & Agami, R. p53-dependent regulation of Cdc6 protein stability controls cellular proliferation. *Mol. Cell. Biol.* **25,** 6937–6947 (2005).
25. Kent, W. J. *et al*. The human genome browser at UCSC. *Genome Res.* **12,** 996–1006 (2002).

nature cell biology

DOI: 10.1038/ncb2105

Figure S1a

M	A	P	primaryAccession	description
0.061836	9.61413	0.23458	11023	hsa-miR-222|rno-miR-222|mmu-miR-222

M	A	P	primaryAccession	description
0.191585	7.81673	0.24234	11022	hsa-miR-221|rno-miR-221|mmu-miR-221

Figure S1b

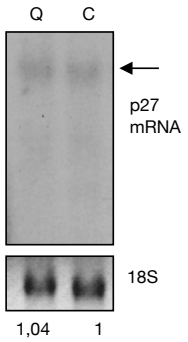

Figure S1c

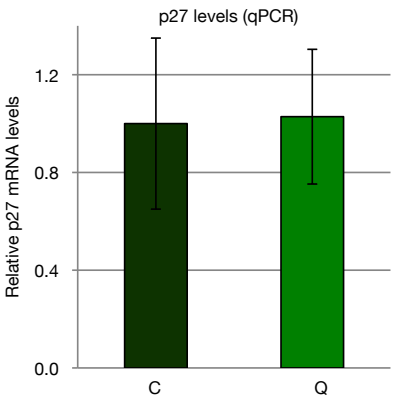

Figure S1d

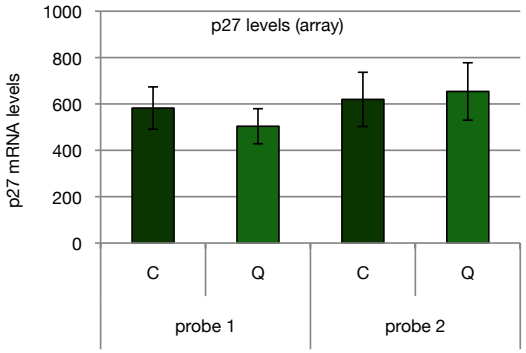

Figure S1e

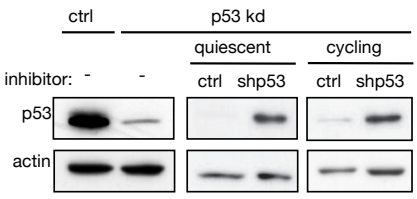

Figure S1 MiR-221/222 and p27 levels in quiescent (Q) versus cycling (C) cells. (**a**) MiR-221 and miR-222 expression analysis on the Exiqon v2 microRNA microarray platform. M represents fold change (log2) as detected in quiescent versus cycling BJ cells. Hybridization was performed using a standard protocol (http://microarrays.nki.nl). (**b**) Northern blot for p27 mRNA and ethidium bromide staining for 18S ribosomal RNA in quiescent versus cycling BJ cells. Densitometric analysis resulted in the normalized amounts displayed below. (**c**) The amount of p27 mRNA was measured by qRT-PCR in cycling and quiescent BJ cells. Error bars represent SD from triplicate reactions. (**d**) Expression analysis of p27 on the Illumina Sentrix BeadChip v3 microarray platform. Absolute expression values were obtained with two probes in quiescent versus cycling BJ cells. The data is a representative of a duplo experiment. Hybridization was performed using a standard protocol (http://microarrays.nki.nl). (**e**) An antago-p53kd was administered to quiescent and cycling BJ-p53kd cells and immunoblot analysis on BJ-p53kd and control cells was performed with p53 and actin control antibodies.

Figure S2a

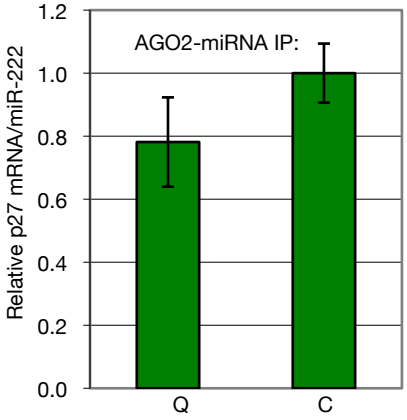

Figure S2b

Enrichment in AGO2 IP/CDK4 IP

	C	+/-		C	+/-
p27	**4.9**	2.1	p27	**3.2**	0.5
miR-221	**8.3**	0.9	miR-222	**3.7**	0.5
gapdh	**1.4**	0.1	gapdh	**1.2**	0.4

Figure S2c

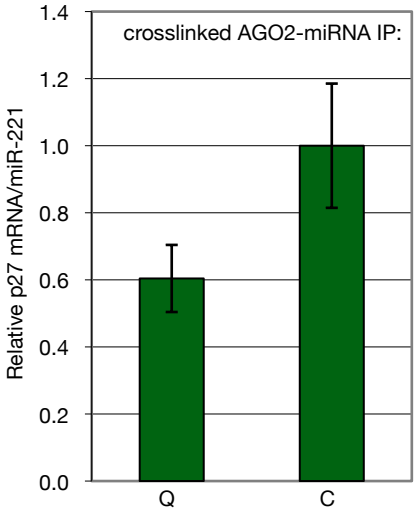

Figure S2d

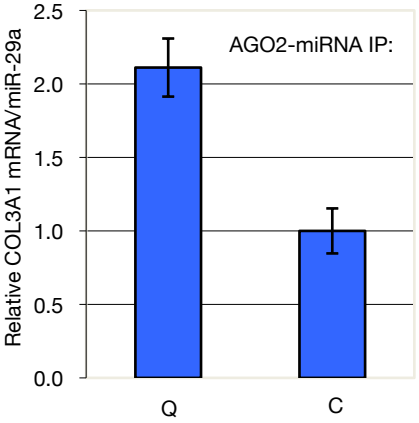

	C	+/-
p27	**4.7**	1.3
miR-221	**5.0**	0.7
gapdh	**1.0**	0.2

Figure S2 Relative amounts of miRNAs and associated mRNAs in AGO2 IPs. (**a**) The amounts of miR-222 and p27 mRNA were measured by qRT-PCR in the IPs shown in Fig. 1e. Results are presented as relative p27/miR-222 ratio. The ratio in the IPs from cycling BJ cells was set to 1. Error bars represent SEM from triplicate reactions. (**b**) Enrichment factors and SEM of miR-221, miR-222, p27 and gapdh control mRNA in AGO2 IPs over CDK4 IPs. (**c**) qRT-PCR performed as in **a,** for miR-221 and p27 mRNA in AGO2 IPs from formaldehyde crosslinked BJ cells. Enrichment factors and SEM of miR-221, p27 and gapdh control mRNA in AGO2 IPs over CDK4 IPs are shown in the table. (**d**) qRT-PCR performed as in **a** for miR-29a and COL3A1 mRNA.

Figure S3a

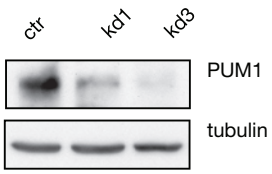

Figure S3b

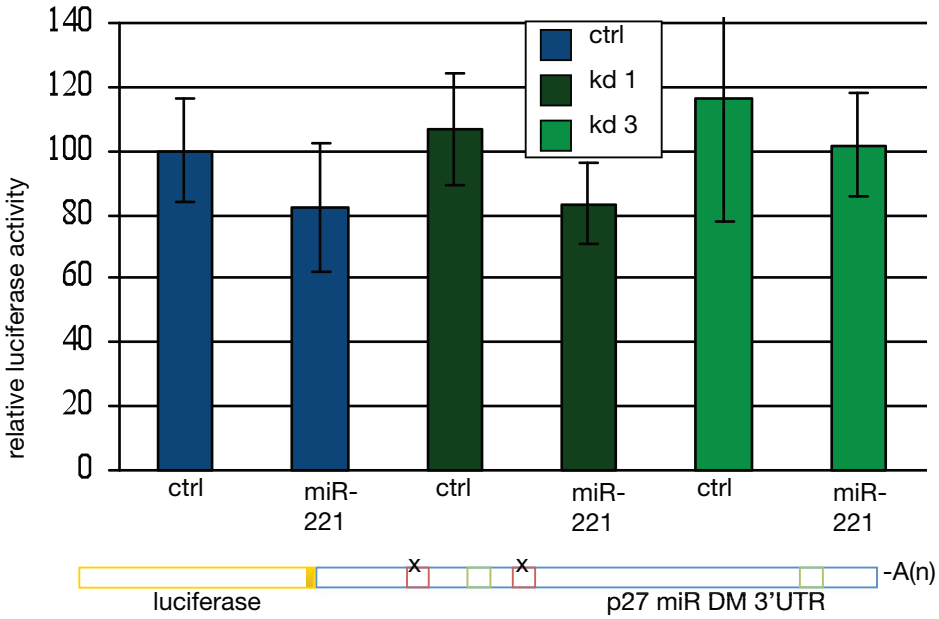

Figure S3 Effect of PUM1 knockdown on miR-221 mediated regulation towards the p27-3'UTR. (**a**) MCF7 cells were transfected with shRNA vectors against PUM1 or control and selected, immunoblot analysis was performed with PUM1 and tubulin control antibodies. (**b**) Luciferase assay performed as in Fig. 2c, with a luciferase construct coupled to the p27-3'UTR mutated for the miR-221/222 sites. Error bars represent SD from three independent experiments.

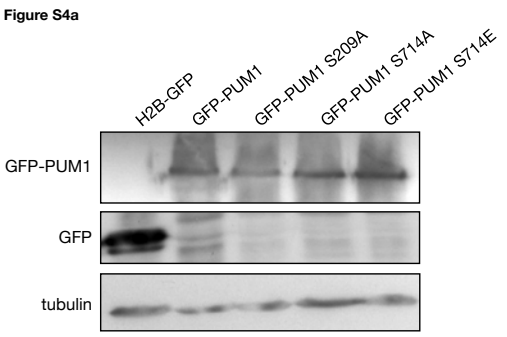

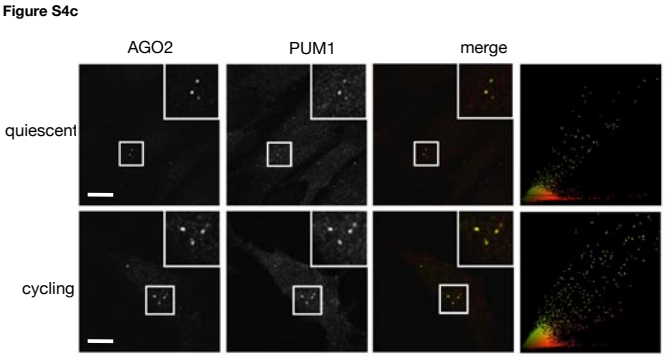

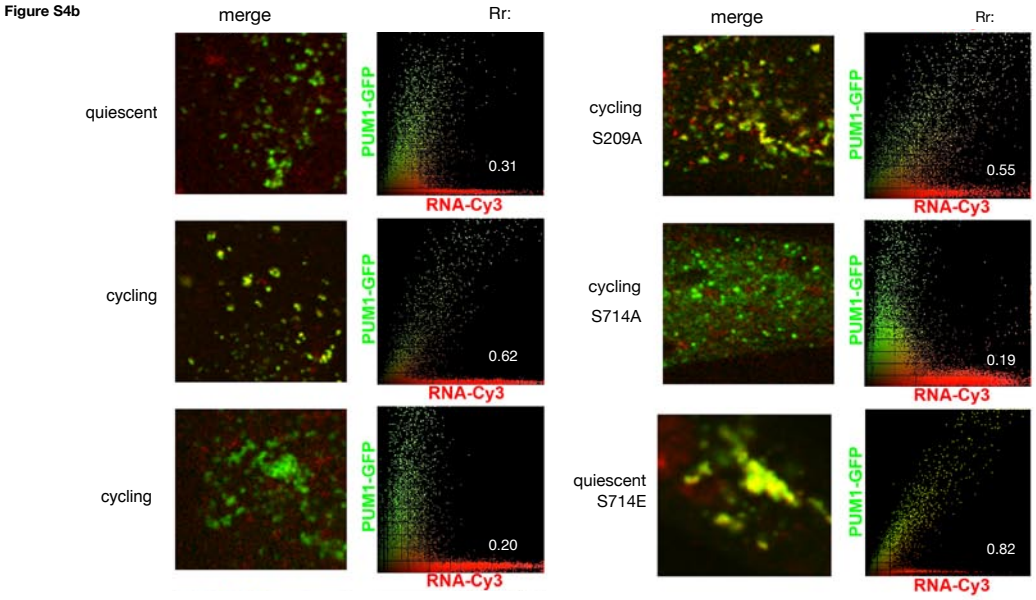

Figure S4 Localization and expression level analysis of PUM1 and control RBPs. (**a**) Confirmation of expression levels of GFP-PUM1 constructs by immunoblot for GFP and tubulin. (**b**) Zoom-in of the inset in merge panel and scatterplots in Fig. 3a,f,g. (**c**) Immunostaining for endogenous PUM1 and AGO2 in quiescent and cycling BJ cells. Colocalisation analyses within the same cell were performed through a scatter plot. Inset shows zoom-in on the highlighted area. Scalebar represents 10 μm. Representative pictures are shown. (**d**) Cycling BJ cells were microinjected with GFP-RBP control constructs and a Cy3-labeled RNA as in Fig. 3a. Representative pictures are shown. (**e**) Confirmation of expression levels of GFP-PUM1HD and GFP-RBP constructs by immunoblot for GFP and tubulin. (**f**) Quantification of RPA signals as shown in Fig. 3c, quantifications were performed with Phosphoimager software. (**g**) Quiescent or cycling BJ cells were microinjected with the GFP-PUM1HD construct and a Cy3-labeled RNA as in Fig. 3a. Representative pictures are shown.

Figure S4d

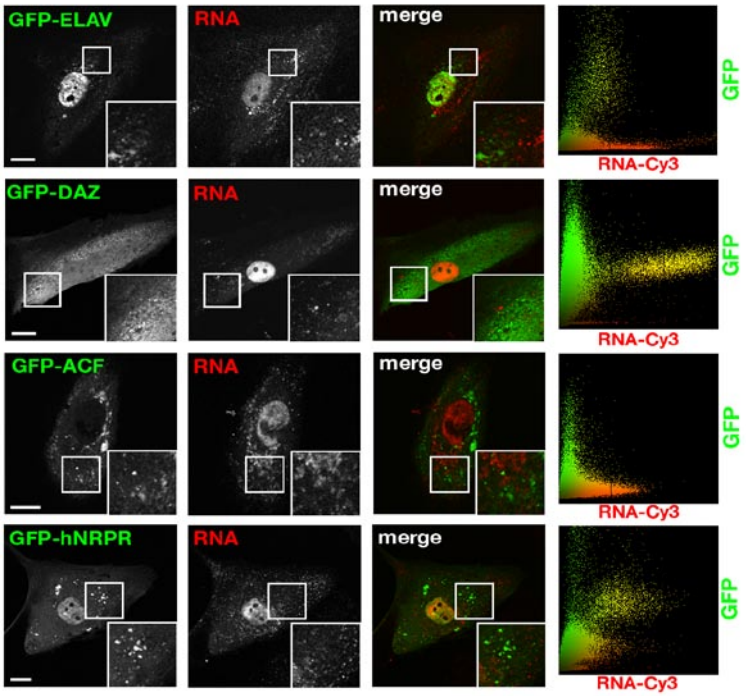

Figure S4e

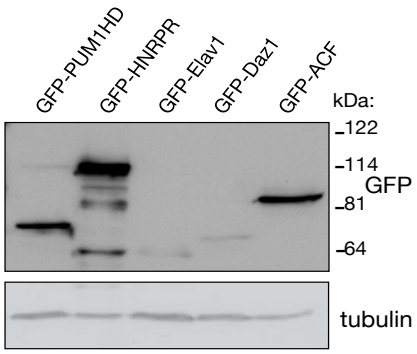

Figure S4f

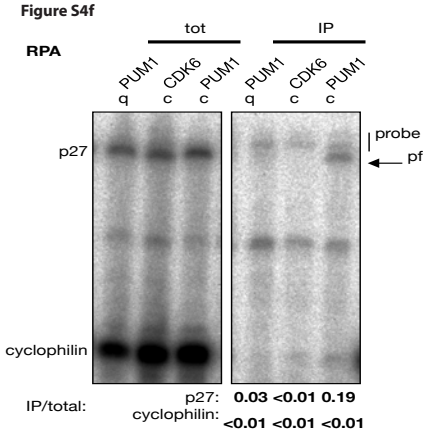

Figure S4g

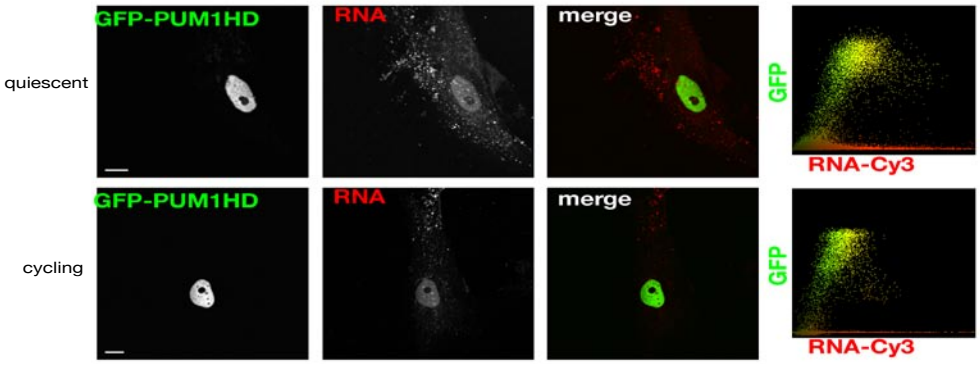

Figure S4 continued

Figure S5a

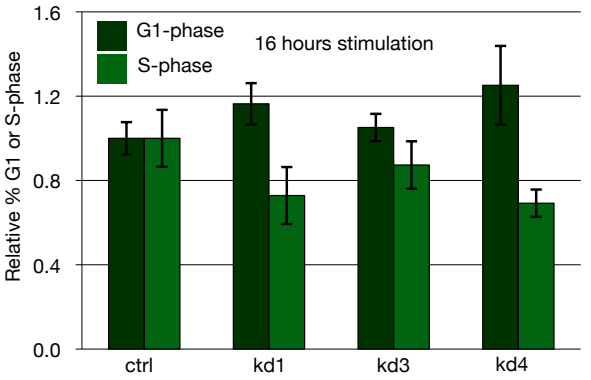

%	ctrl	PUM1 kd1	PUM1 kd3	PUM1 kd4
G1	62.0	71.9	65.0	77.2
S	33.9	24.4	29.4	23.4
G2/M	2.9	3.0	3.6	2.7

Figure S5b

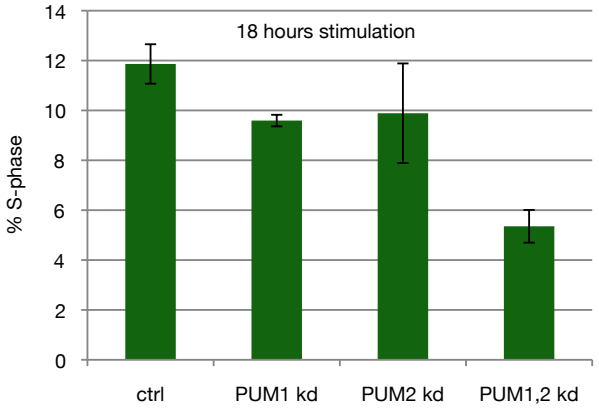

%	ctrl	PUM1 kd	PUM2 kd	PUM1,2 kd
G1	73.1	74.2	76.2	79.5
S	11.9	9.6	9.9	5.4
G2/M	14.8	16.0	13.4	14.4

Figure S5c

	%	ctrl	PUM1,2 kd
wt	G1	84.5	85.1
	S	6.5	3.0
	G2/M	8.4	11.3
p27 kd	%	ctrl	PUM1,2 kd
	G1	86.1	85.3
	S	7.7	7.1
	G2/M	5.8	7.2

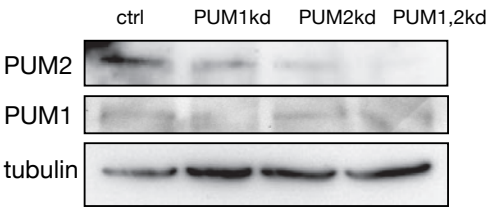

Figure S5 Loss of Pumilio affects cell cycle progression. (**a**) BJ cells containing stable PUM1 knockdowns or control were growth factor deprived and then stimulated for 16 hours with growth factors. The percentage of cells in S-phase was determined by flow cytometric analysis of BrdU incorporation. G1- and G2/M- phase percentages as measured by propidium iodine are shown below. Error bars represent the SD of triplicate experiments. (**b**) BJ cells were transfected with either siPUM1, siPUM2, both, or control siRNA, and growth factor deprived for 72 hours. After 18 hours of subsequent growth factor stimulation, the percentage of cells in S-phase was determined by flow cytometric analysis of BrdU incorporation. G1- and G2/M- phase percentages as measured by propidium iodine are shown below. Error bars represent the SD of triplicate experiments. Immunoblot analysis of quiescent BJ cells stimulated with growth factors for PUM1&2 and tubulin control. (**c**) G1- and G2/M- phase percentages as measured by propidium iodine from Fig. 4d.

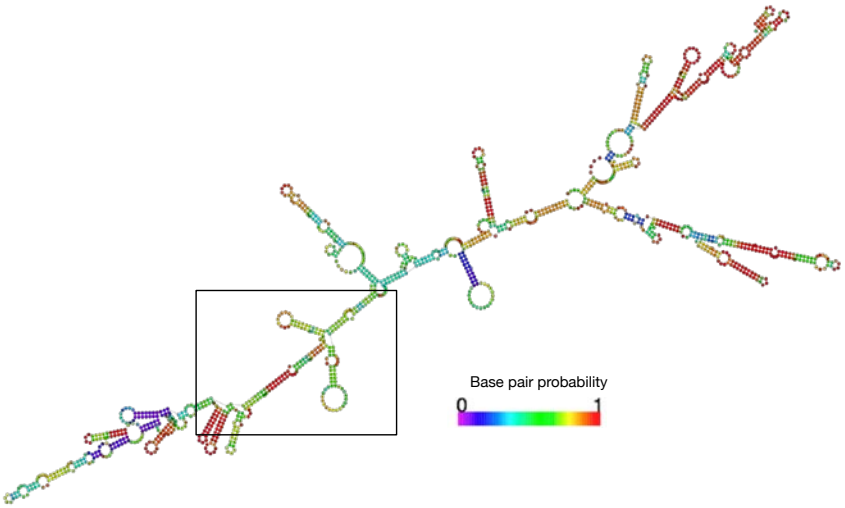

Figure S6 Predicted conformation of the complete p27-3'UTR**.** A schematic representation of the conformation of the complete p27-3'UTR as predicted by RNAfold software. Base pair probability is indicated in the legend.

Figure S7a

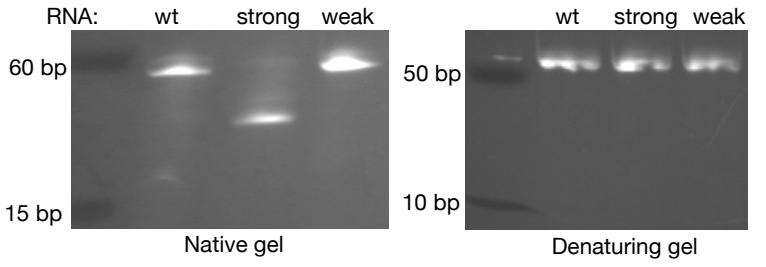

Figure S7b

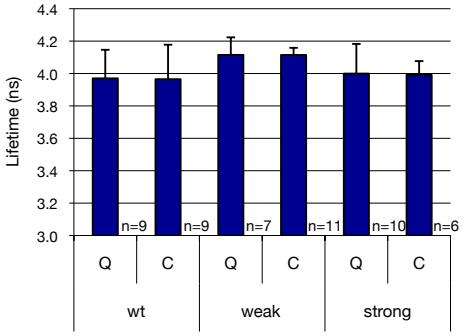

Figure S7 Conformation of tagged RNA oligos and single labelled FLIM control. (**a**) Gel migration analysis of RNA oligos containing wildtype, strong and weak mutant p27-3'UTR-PRE and the proximal miR-221/222 binding site. (**b**) Quiescent (Q) and cycling (C) BJ cells were microinjected with short RNAs containing the p27-3'UTR-PRE and the proximal miR-221/222 binding site, and tagged with 3' (fluorescein) fluorophore. The wildtype, weak and strong mutants described in the text were used. Cy3 fluorophore lifetimes (in ns) due to FRET are displayed. Error bars represent SD.

Figure S8

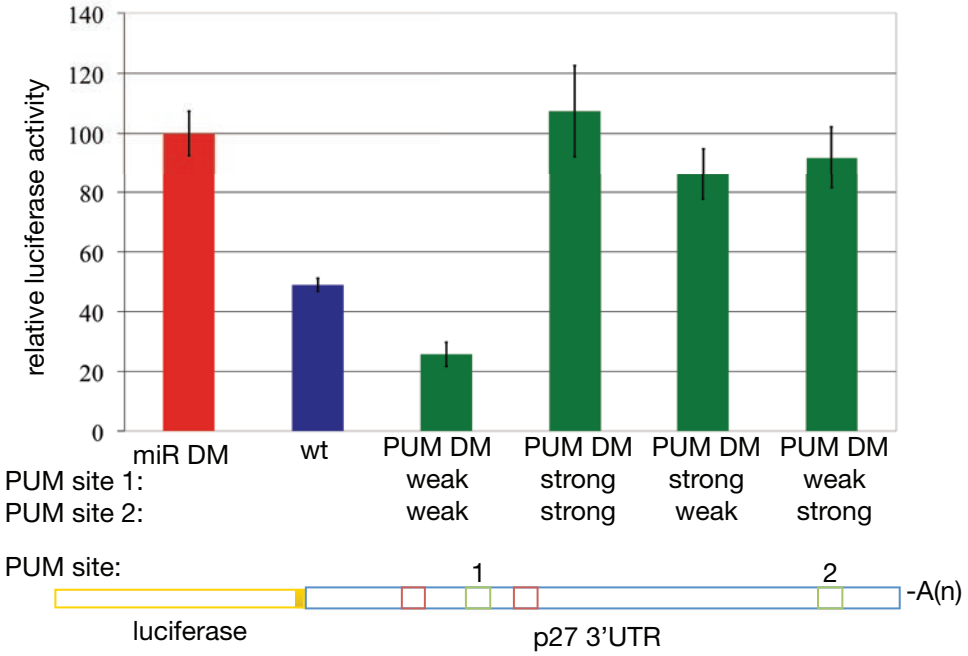

Figure S8 Functional interaction between Pumilio and miRNA sites in the p27-3'UTR. Luciferase assay performed as in Fig. 2c, in HEK293 cells (endogenously expressing miR-221/222), with luciferase constructs coupled to the p27-3'UTR mutated for the miR-221/222 sites (miR DM), and several constructs mutated for both Pumilio sites (see schematic representation below). Pumilio sites 1 and 2 are shown in green, miRNA-221/222 sites are shown in red, weak and strong PUM site mutants are as described in the text. Error bars represent SD from three independent experiments.

Figure S9a

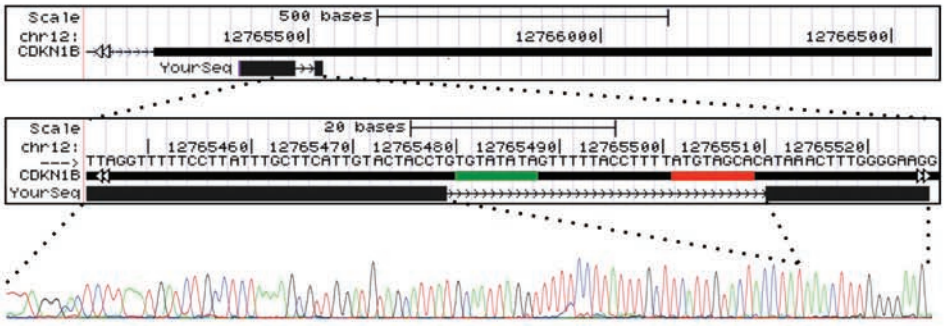

Figure S9b

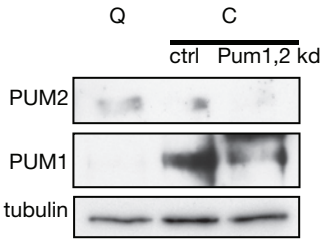

Figure S9 In vivo crosslinking reveals predicted secondary p27-3'UTR structure. (**a**) Schematic representation of the bridge PCR product (yourseq) adapted from BLAT search function [23] with nucleotide numbers shown. Sequence is shown below, as expected the miR-221/222 site (red) and the Pumilio site (green) are missing from the PCR product. (**c**) Immunoblots showing levels of PUM1&2 and control tubulin from crosslinked BJ cells from Fig. 5d.

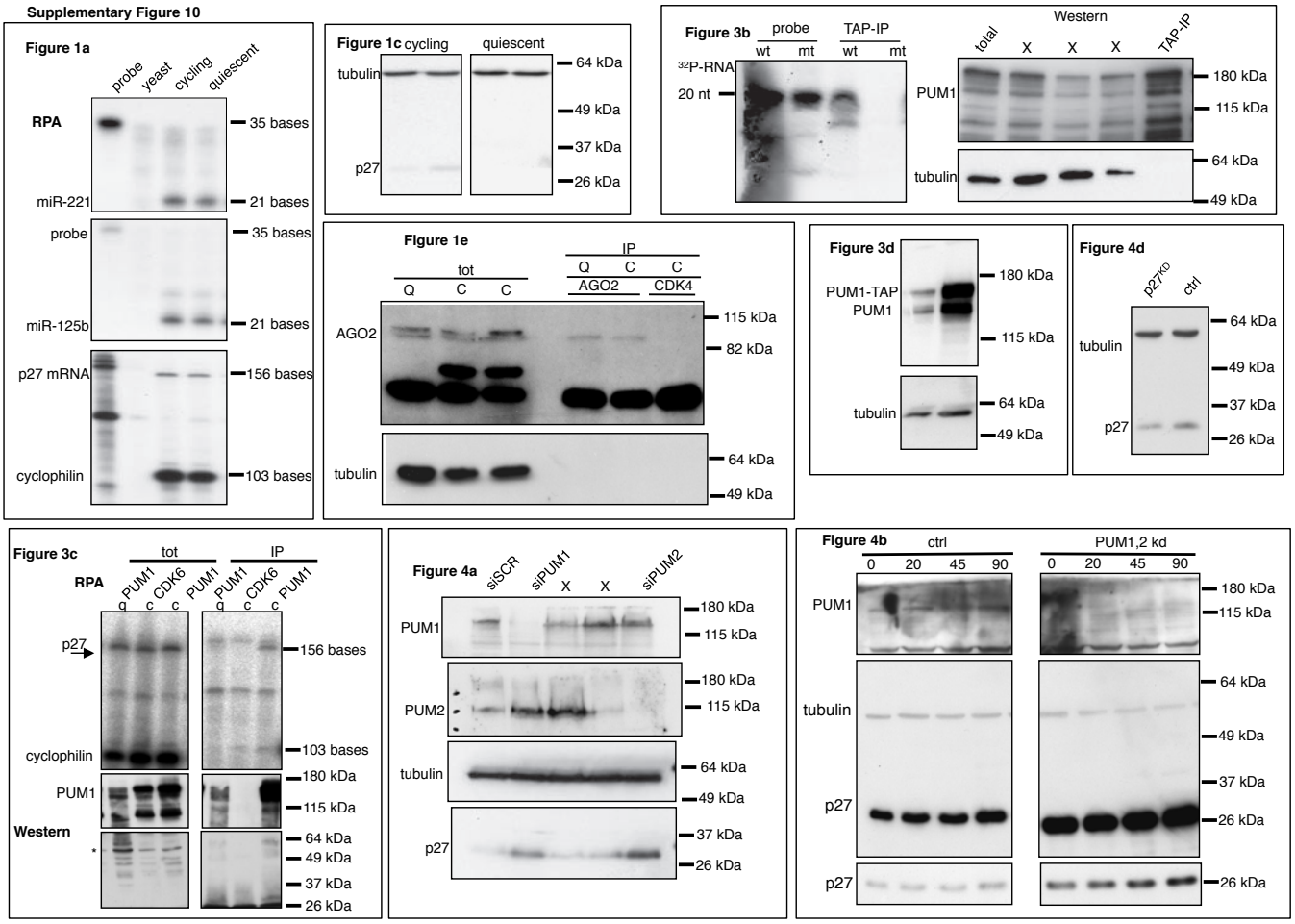

Figure S10 Full scans